Power System Technology **Volume 46 · Number 1 · 2022**
ISSN: 1000-3673

Electricity Retail Side Market Framework Design in National Unified Electricity Market System

Yuan H., Dong X., Liu Q., Jin L., Zhang W., Yang Z.
1. College of Engineering and Technology, American University of the Middle East, Kuwait
2. Faculty of Science III, Lebanese University, Lebanon

ABSTRACT
This paper presents the design, simulation, and analysis of different 3D-shapes of scanning near-field optical microscopy probes, allowing the acquisition of both topographic and optical images. The study is conducted using COMSOL and ANSYS simulation tools to study the probe sensitivity and deflection. The simulation calculations of deflection and von Mises stress are denoted, analyzed, and compared based on the change in the probe shapes for the same applied force. The results obtained from the two finite element tools were similar, converged to the same ideal design, and showed the impact of the probe structure on the probe performance.

1. INTRODUCTION

Most commercial probes used in scanning near-field optical microscopy (SNOM) are based on tapered optical fibers and can work in emission and collection modes [1]. This type of probe has low-cost fabrication but is hardly reproducible and fragile. Cantilever-type SNOM probes are advantageous compared to tapered optical fibers (batch fabrication, better mechanical resistance, possibility of optical function integration) but can work only in the emission mode (hollow tip). A transmission of approximately 10^{-3} to 10^{-5} was obtained [2-4]. A new cantilever-type SNOM probe has been proposed in a previous study [5] collecting the advantages of all commercial SNOM probes, offering the opportunity to work in emission and collection mode and therefore enables the acquisition of both optical and topographic images, which is not the case for any commercial SNOM probe. A 2D simulation study using COMSOL Multiphysics was performed based on the calculation of the optical transmission coefficient in both emission and collection modes, allowing the prediction of the optimal geometrical probe parameters (cantilever thickness, tip, and tip apex dimensions). However, the mechanical properties and probe sensitivity of this new type of SNOM probe have not been investigated. Many research papers highlighted the importance of the design structure on the mechanical properties [6-8]. Some other works used numerical simulation tools in their studies especially when dealing with nontrivial geometries [9-11]. In this paper, taking into consideration the optimal probe dimensions obtained previously and providing a higher transmission coefficient, we present a 3D simulation study showing the impact of the probe structure and the importance of the cantilever design on the probe sensitivity, and therefore on the probe performance. 3D simulations are more realistic and offer the possibility of visualizing the stress distribution all over the probe structure, which facilitates the analysis of the results and leads to an ideal design. However, this was not the case in the 2D simulation.

Simulations were carried out using two different finite element analysis tools: COMSOL Multiphysics and ANSYS. Different microcantilever-type probe designs were proposed, in which the deflection was calculated for each design for the same amount of force applied. The total displacement or deflection was measured by fixing one end of the cantilever probe, and the other end was free to move when it experienced force. The von Mises stress was also calculated for each design. The results obtained in COMSOL and ANSYS are compared to validate the study and to choose the best design that prompts the greatest cantilever probe flexibility.

The cantilever probe behavior can be explained by Equations (1) and (2), which indicate that the cantilever deflection δ is directly proportional to the applied stress σ and depends on the force applied F, cantilever spring constant κ, cantilever probe dimensions (length L, width W, thickness t) and probe material properties (Poisson ratio ϑ, Young modulus E).

$$\delta = \frac{3\sigma(1-\vartheta)}{E}\left(\frac{L}{t}\right)^2 \tag{1}$$

$$\kappa = \frac{F}{\delta} = \frac{EWt^3}{4L^3} \tag{2}$$

2. STUDY PARAMETERS

The probe tip has a pyramidal shape and similar width W to that of the cantilever at the junction tip cantilever. Its height h is 10μm, which is the average height of commercial probes and corresponds to a pyramidal tip width W of 14.14μm. A tip height of 20μm corresponds to 28.28μm width [12,13]. The tip aperture diameter a at its apex and the tip opening angle were set to 50nm and 70.53°, respectively, based on fabrication constraints. Four different probe models were proposed (Figures 1 - 4) with the dimensions given in Table 1.

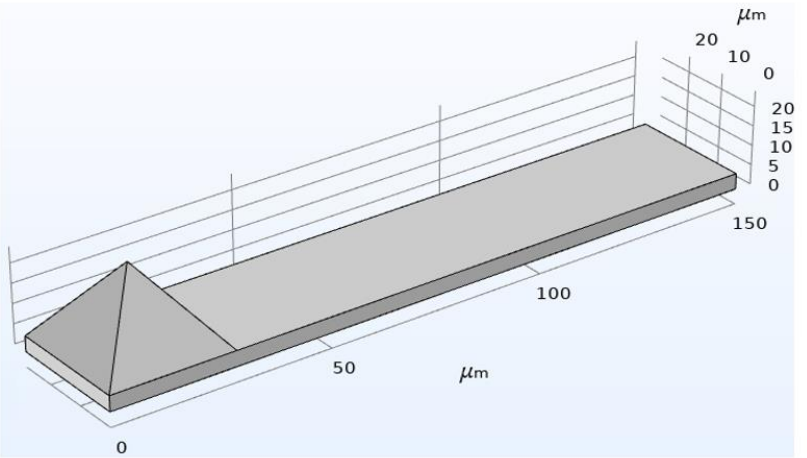

Figure 1: Probe model 1 with a rectangular cantilever shape

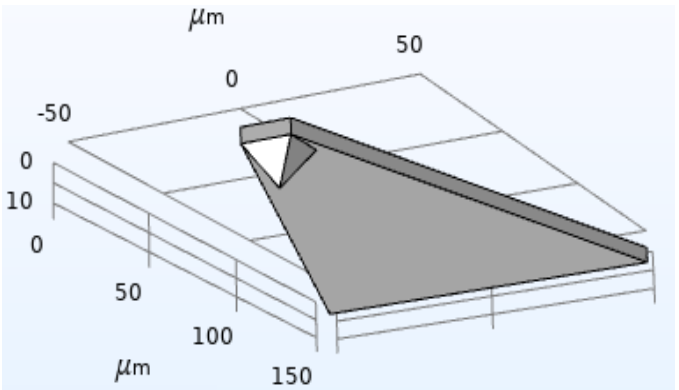

Figure 2: Probe model 2 with a triangular cantilever shape

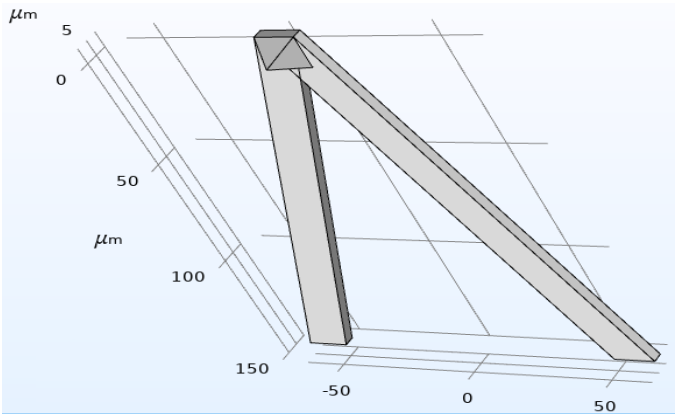

Figure 3: Probe model 3 with a V cantilever shape of width 14.14 μm

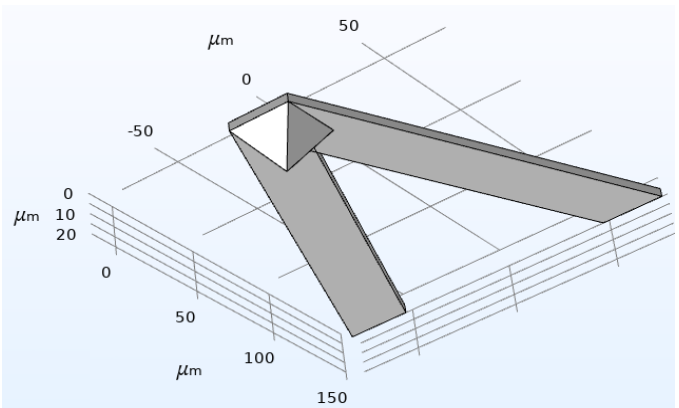

Figure 4: Probe model 4 with a V cantilever shape of width 28.28 μm

Table 1: Probe Models Dimensions

Probe sensor model	Cantilever shape	Tip height h (µm)	Cantilever free end width W (µm)	Cantilever fixed end width W (µm)
1	Rectangular	20	28.28	28.28
2	Triangular	10	14.14	100
3	V	10	14.14	128.28
4	V	20	28.28	156.56

In the four probe models presented above, the cantilever thickness t and tip apex aperture corresponded to 4 µm and 50 nm, respectively. Model 1 probe sensor consists of a rectangular box cantilever shape of width 28.28µm with a tip attached to its free end having the same width and a 20µm height. Model 2 consists of a triangular cantilever shape with free and fixed end widths of 14.14µm and 100µm, respectively. The tip width at the junction with the cantilever is 14.14µm. Probe models 3 and 4 consist of two connected hexahedrons in a V shape with internal edges separated by 100µm. The two connected hexahedrons have the same width W (14.14µm in model 3 and 28.28µm in model 4) at both free and fixed ends with a tip of height h (10µm in model 3 and 20µm in model 4) connected to the probe free end.

The probe structures were made of a polymer material, polymethylmethacrylate (PMMA), with the mechanical properties displayed in Table 2. This material is transparent (ensuring optical image acquisition), dimensionally stable, and rigid. The force applied to the probe free end at the tip location toward the positive y-axis is estimated to be 20nN [14] in the intermittent contact mode.

Table 2: Probes Material Properties

Density (kg/m^3)	Young's Modulus (Pa)	Poisson's Ratio
1190	3E9	0.4

Solid mechanics interface from the structural mechanics COMSOL module was used to calculate the von Mises stress applied on the probe and the cantilever deflection. The simulation is completed and performed at ambient temperature in stationary mode. A user-controlled mesh is defined for the entire geometry using automatic tessellation mode. A free tetrahedral adaptive mesh is defined, with a minimum element size of 32nm. The maximum element growth rate was set to 1.2 with a curvature factor of 0.3.

The static structural ANSYS module is used to calculate the von Mises stress applied to the probe and cantilever deflection. The simulation is completed and performed at ambient temperature in mechanical physics reference mode. A free tetrahedral adaptive mesh is defined, with a minimum element size of 32 nm. The maximum element growth rate is set to 1.2 with a transition ratio of 0.27.

3. SIMULATION RESULTS

Schematic diagrams of all proposed models are shown when a force of 20nN is applied to the free end of the probe at the tip location. In each studied model, simulation results plots for the von Mises stress and probe deformation are introduced separately for both ANSYS (Figures 5 - 12) and COMSOL (Figures 13 - 20) tools.

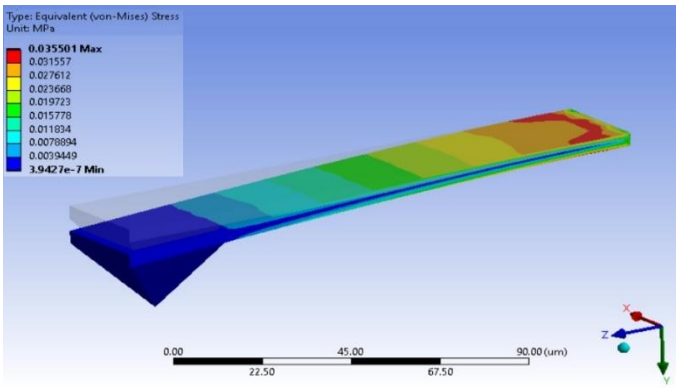

Figure 5: Model 1 (rectangular shape) simulation result plot of Von mises stress illustrating the probe deformed shape.

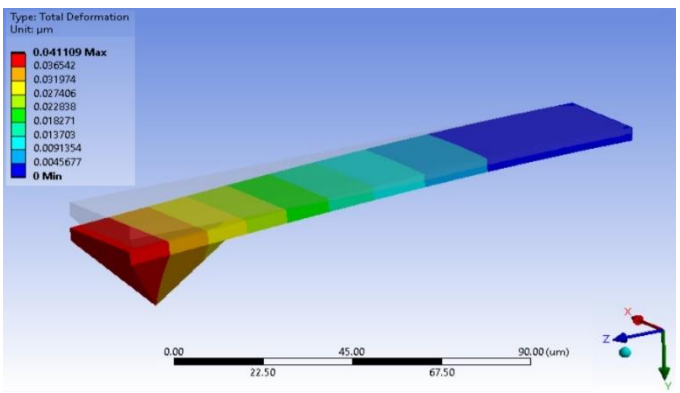

Figure 6: Model 1 (rectangular shape) simulation result plot of probe deflection illustrating the probe deformed shape.

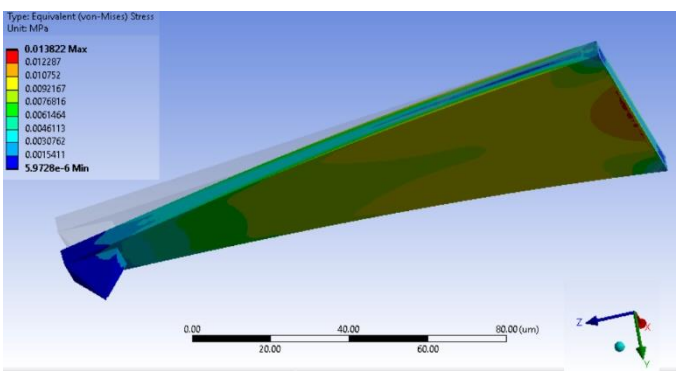

Figure 7: Model 2 (triangular shape) simulation result plot of Von mises stress illustrating the probe deformed shape.

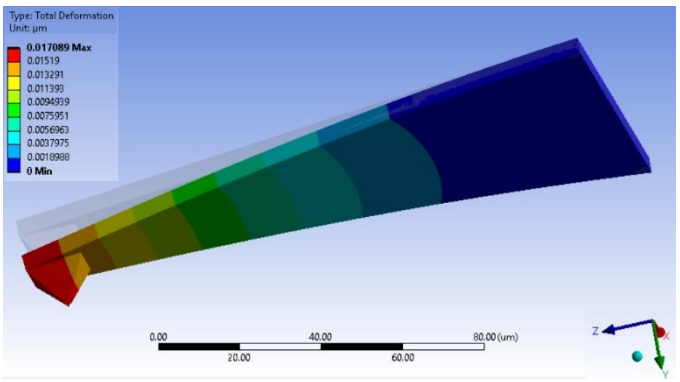

Figure 8: Model 2 (triangular shape) simulation result plot of probe deflection illustrating the probe deformed shape.

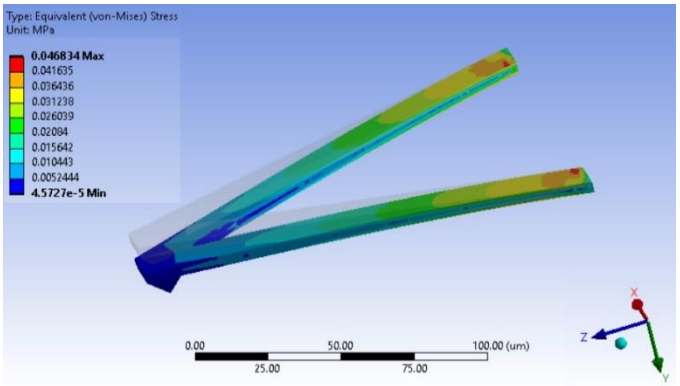

Figure 9: Model 3 (V shape) simulation result plot of Von mises stress illustrating the probe deformed shape.

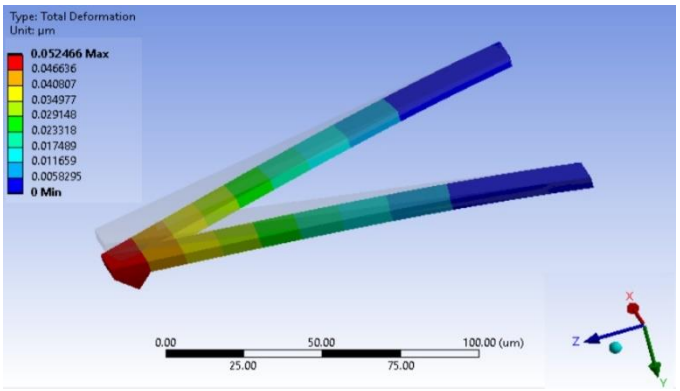

Figure 10: Model 3 (V shape) simulation result plot of probe deflection illustrating the probe deformed shape.

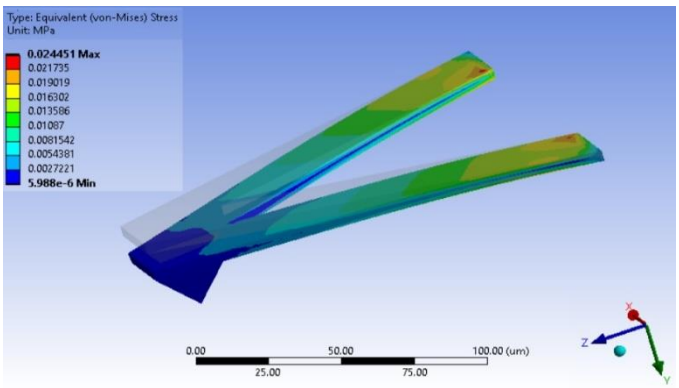

Figure 11: Model 4 (V shape) simulation result plot of Von mises stress illustrating the probe deformed shape.

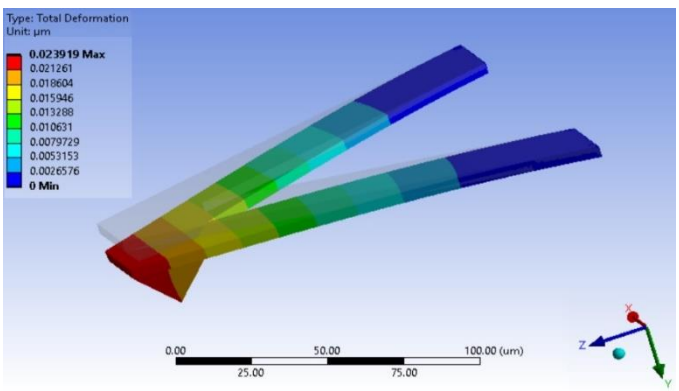

Figure 12: Model 4 (V shape) simulation result plot of probe deflection illustrating the probe deformed shape.

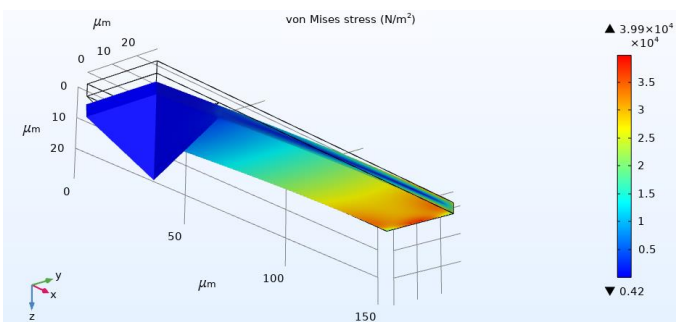

Figure 13: Model 1 (rectangular shape) simulation result plot of Von mises stress illustrating the probe deformed shape.

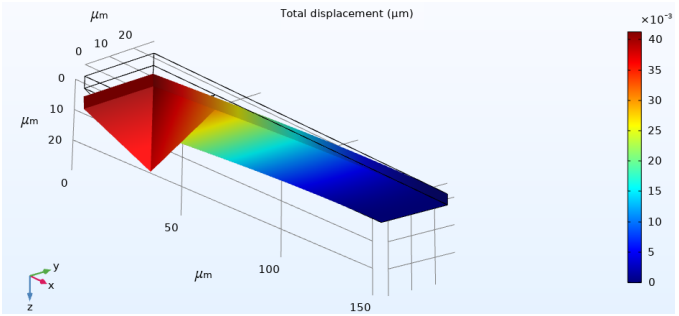

Figure 14: Model 1 (rectangular shape) simulation result plot of probe deflection illustrating the probe deformed shape.

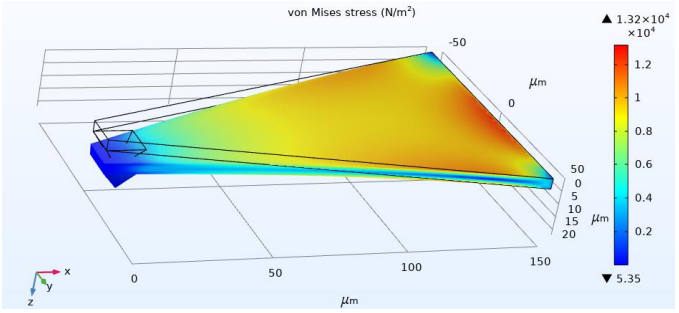

Figure 15: Model 2 (triangular shape) simulation result plot of Von mises stress illustrating the probe deformed shape.

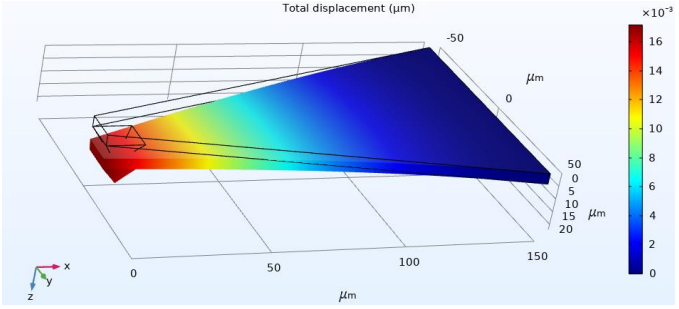

Figure 16: Model 2 (triangular shape) simulation result plot of probe deflection illustrating the probe deformed shape.

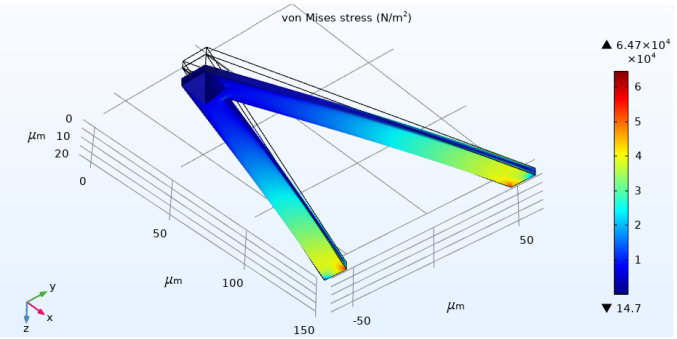

Figure 17: Model 3 (V shape) simulation result plot of Von mises stress illustrating the probe deformed shape.

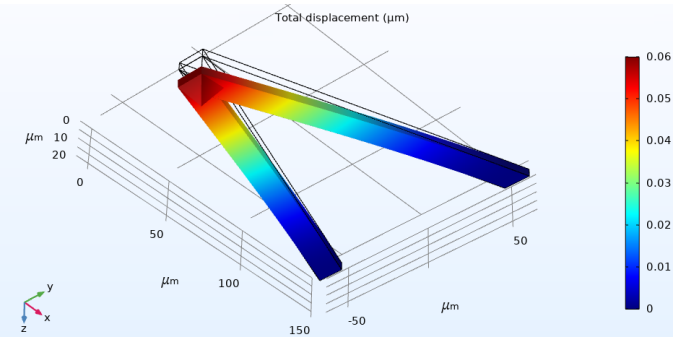

Figure 18: Model 3 (V shape) simulation result plot of probe deflection illustrating the probe deformed shape.

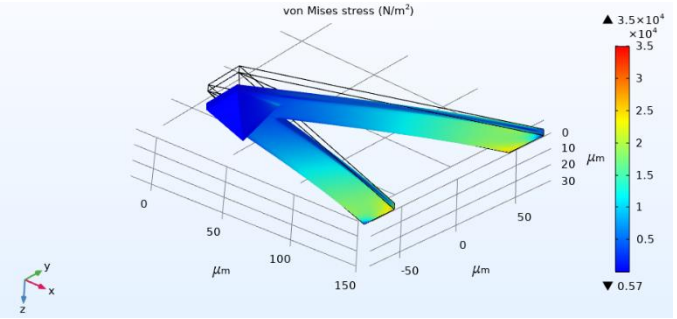

Figure 19: Model 4 (V shape) simulation result plot of Von mises stress illustrating the probe deformed shape.

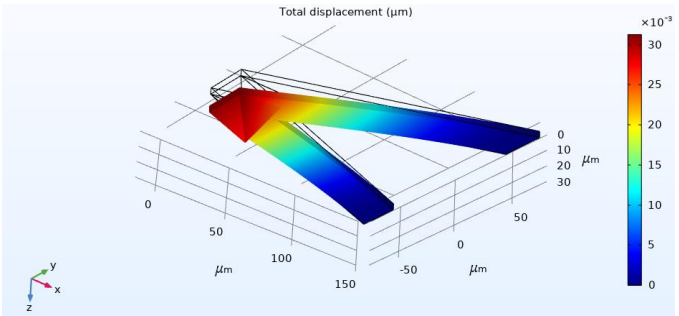

Figure 20: Model 4 (V shape) simulation result plot of probe deflection illustrating the probe deformed shape.

Table 3: COMSOL-ANSYS Comparison Table Results

Probe sensor model	**Von mises stress (x10^3 N/m^2)**		**Probe free end Deflection (x10^{-3} µm)**	
	COMSOL	**ANSYS**	**COMSOL**	**ANSYS**
1	22.59	35.5	41.33	41.1
2	13.64	13.82	17.19	17.08
3	53.9	46.83	60	52.46
4	26.4	24.45	31.31	23.91

To analyze the results, the von Mises stress and deflection maximum values obtained for each model are presented in Table 3 for both COMSOL and ANSYS tools.

From the above schematics, the stress applied to the probe is mainly concentrated at its fixed end. In models 1 and 2, the stress is distributed more at the center of the cantilever fixed end than on the edges. Nonetheless, in models 3 and 4, more stress is applied to the tetrahedral internal edges. The minimum estimated stress value was obtained in model 2, which corresponds to the highest structure surface. The stress is then appropriated all over the surface and takes a minimum value. This analysis is valid for both the COMSOL and ANSYS simulation tools. Likewise, one can see the probe deformation in all models and for both simulation tools at the probe-free end location. This is evident because the force is applied on the probe tip towards the positive y-axis; thus, the probe deflects down. The minimum measured deflection value is also obtained in model 2, which is rational because the minimum stress is measured in this model.

Comparing the COMSOL and ANSYS simulation tools, the maximum deflection and stress values obtained are almost similar for the same model (Table 3) and are comparable between the models. One can notice that the model 3 probe sensor structure (V shape of 14.14µm width) has greater sensitivity compared to all other presented models when the same amount of force is applied on each of them. Subsequently, model 3 presents the ideal probe structure choice among the other models as it ensures the highest deflection.

4. CONCLUSION

Commercial SNOM probes (tapered optical fibers or cantilever type) available in the market allow the use of this microscopy in either the emission or collection mode. A new type of probe cantilever-based type has been presented in a previous paper (2D simulation), collecting the advantages of commercial probes, and offering the possibility of working in the emission and collection mode. Probe sensitivity is a crucial factor that directly affects probe performance. In this study, the effect of the probe structure on probe sensitivity was studied. Different SNOM probe structures were designed in 3D, and their sensitivity was investigated when the same amount of force was applied to the free-end probe tip. These probes are made of transparent polymer materials that permit the acquisition of both topographic and optical images. The impact of the probe sensor structure on probe performance was studied by calculating the von Mises stress and probe deflection. The proposed probe models had similar cantilever thicknesses and tip apex apertures. Two different finite element tools were used in this study: COMSOL and ANSYS. It is tracked down that both methods converge to the same findings showing that the V shape probe model (model 3) is the ideal probe sensor structure as it has the greater sensitivity. This result requires an additional 3D simulation study of the optical transmission in both emission and collection modes using the same presented designs. This will be investigated in a future study.

CONFLICTS OF INTEREST

The authors declare no conflict of interest.

REFERENCES

[1] M. Labardi, P. G. Gucciardi, and M. Allegrini, “Near-field optical microscopy,” La Rivista del Nuovo Cimento, vol. 23, no. 4, pp. 1–35, Apr. 2000.

[2] M. Salomo, D. Bayer, B. R. Schaaf, M. Aeschlimann, and E. Oesterschulze, “Fabrication and characterization of coaxial scanning near-field optical microscopy cantilever sensors,” Microelectronic Engineering, vol. 87, no. 5–8, pp. 1540–1542, May 2010.

[3] L. Wang and X. Xu, “High transmission nanoscale bowtie-shaped aperture probe for near-field optical imaging,” Applied Physics Letters, vol. 90, no. 26, p. 261105, Jun. 2007.

[4] W. S. Chang, S. Bauerdick, and M. S. Jeong, “Resolution enhancing using cantilevered tip-on-aperture silicon probe in scanning near-field optical microscopy,” Ultramicroscopy, vol. 108, no. 10, pp. 1070–1075, Sep. 2008.

[5] B. Mourched, E. L. Nativel, R. Kribich, P. Falgayrettes, and P. Gall-Borrut, “Study of light emission and collection in a transparent dielectric cantilever-based near-field optical probe,” Journal of Microscopy, vol. 262, no. 1, 2016.

[6] Paulls, A., Sun, D. and Swift, K. (2007) “Stress Concentrations Optimisation Process for Engineering Structures”, The International Journal of Multiphysics, vol. 1, no. 2, pp. 175-188.

[7] G. Acciani, A. Dimucci, and L. Lorusso, “Multimodal piezoelectric devices optimization for energy harvesting,” The International Journal of Multiphysics, vol. 7, no. 3, pp. 227–244, Sep. 2013.
[8] H. Khawaja, “Application of a 2-D approximation technique for solving stress analyses problem in FEM,” International Journal of Multiphysics, vol. 9, no. 4, pp. 317–324, Dec. 2015.
[9] D. Brunner, H. Khawaja, M. Moatamedi, and G. Boiger, “CFD modelling of pressure and shear rate in torsionally vibrating structures using ANSYS CFX and COMSOL Multiphysics,” The International Journal of Multiphysics, vol. 12, no. 4, pp. 349–358, Dec. 2018.
[10] M. Jourdani, H. Mounir, and A. Marjani, “Three-Dimensional PEM Fuel Cells Modeling using COMSOL Multiphysics,” The International Journal of Multiphysics, vol. 11, no. 4, pp. 427–442, Dec. 2017.
[11] Parkhe et al., “Analytical and Numerical Stress Analysis of Composite Box Beam in Dynamic condition and Validation with COMSOL Multiphysics software”, Aegaeum journal, vol. 8, no. 4, pp. 380–387, May. 2020, ISSN: 0776-3808
[12] G. Schürmann et al., "Fabrication and characterization of a silicon cantilever probe with an integrated quartz-glass (fused-silica) tip for scanning near-field optical microscopy," Appl. Opt. vol. 40, no. 28, pp. 5040-5045 (2001).
[13] G. Schürmann, P. F. Indermühle, U. Staufer, N. F. de Rooij, “Micromachined SPM probes with sub-100 nm features at tip apex,” Surface and Interface Analysis, vol. 27, issue 5-6, pp. 299–301, June. 1999.
[14] Anczykowski, D. Krüger, K. L. Babcock, and H. Fuchs, “Basic properties of dynamic force spectroscopy with the scanning force microscope in experiment and simulation,” Ultramicroscopy, vol. 66, no. 3–4, pp. 251–259, Dec. 1996.